BSJ
BURAPHA SCIENCE JOURNAL
ISSN 2985-0983 (online)

วารสารวิทยาศาสตร์บูรพา ปีที่ 31 (ฉบับที่ 1) มกราคม – เมษายน พ.ศ. 2569

BURAPHA SCIENCE JOURNAL Volume 31 (No.1) January – April 2026

Research Article

Mango Leaf Extract–Mediated Silver Nanoparticles for Photocatalytic Degradation of Methylene Blue

Nuttawisit Yasarawan*

Department of Chemistry, Faculty of Science, Burapha University, Thailand

Received : 12 February 2026, Received in revised form : 17 March 2026, Accepted : 24 March 2026

Available online : 30 March 2026

Abstract

Background and Objectives: Silver nanoparticles (AgNPs) have been widely studied owing to their distinctive optical and catalytic properties, which enable applications in antimicrobial treatment, sensing, and environmental remediation. In particular, AgNPs have attracted growing interest as photocatalysts for the degradation of organic dyes in wastewater under light irradiation, due to their strong surface plasmon resonance (SPR) and their ability to promote the formation of reactive oxygen species. Nevertheless, conventional AgNP synthesis methods frequently employ hazardous chemical reducing agents and stabilizers, raising concerns regarding environmental impact, safety, and sustainability. Consequently, green synthesis strategies based on plant-derived extracts have emerged as promising alternatives, utilizing naturally occurring phytochemicals as reducing and stabilizing agents. Mango (Mangifera indica) leaves are an abundant agricultural byproduct in Thailand and contain high levels of polyphenolic compounds, particularly mangiferin, which exhibit strong reducing and antioxidant activities. Despite this potential, systematic studies on the formation kinetics of mango leaf extract (MLE)–mediated AgNPs and their photocatalytic performance under practical, low-energy light sources remain limited. Therefore, this study aimed to develop an environmentally friendly synthesis route for AgNPs using MLE, to investigate the effects of key synthesis parameters on AgNP formation kinetics, and to evaluate the applicability of the synthesized AgNPs for photocatalytic degradation of methylene blue (MB) in aqueous solutions under white LED and solar irradiation.

Methodology: MLE was prepared using deionized water as the sole extraction solvent to ensure a simple, non-toxic, and environmentally benign process compatible with aqueous silver precursor solutions. AgNPs were synthesized via the reduction of Ag^{+} ions from $AgNO_3$ using MLE under systematically varied experimental conditions, including incubation temperature (20–60 °C), $AgNO_3$ concentration (1–7 mM), MLE volume fraction (1–30% v/v), and pH (3–11), in order to elucidate their effects on reduction kinetics, nanoparticle formation, and photocatalyst preparation. The formation of AgNPs was monitored by UV–Vis spectrophotometry through the time-dependent evolution of the SPR absorption band. Kinetic data were analyzed using a pseudo-first-order model, and observed rate constants were obtained by nonlinear curve fitting. Temperature-dependent rate constants were further examined using Arrhenius and Eyring analyses to determine activation energies and thermodynamic activation parameters. The synthesized AgNPs were characterized by Fourier-transform

infrared spectroscopy (FTIR), transmission electron microscopy (TEM), scanning electron microscopy (SEM), X-ray diffraction (XRD), and X-ray fluorescence spectroscopy (XRF) to evaluate functional group involvement, morphology, crystalline structure, and elemental composition. Photocatalytic performance was evaluated by monitoring methylene blue (MB) degradation under white LED irradiation (30 W and 60 W) and natural solar irradiation. The effects of AgNP dosage and initial MB concentration on removal efficiency were systematically investigated, and degradation kinetics were analyzed using a pseudo-first-order model. All photocatalytic experiments were carried out under identical geometric configurations to ensure consistent light exposure. Prior to irradiation, reaction mixtures were magnetically stirred in the dark to establish adsorption–desorption equilibrium between MB molecules and AgNP surfaces. Control experiments conducted in the absence of AgNPs confirmed negligible photolysis of MB under the applied irradiation conditions throughout all experiments.

Main Results: UV–Vis spectrophotometric analysis confirmed successful AgNP formation by the appearance and progressive increase of a characteristic SPR band at approximately 425 nm, accompanied by a visible color change of the reaction mixture from yellow to reddish-brown. The formation kinetics followed a pseudo-first-order model with high coefficients of determination ($R^2 > 0.99$). Increasing incubation temperature resulted in higher observed rate constants, indicating a thermally activated reduction process. Arrhenius and Eyring analyses yielded similar activation energies of approximately 27 kJ mol^{-1}, suggesting efficient reduction of Ag^+ ions by MLE-derived phytochemicals. FTIR spectra revealed a decrease in O–H stretching intensity along with both an increase in intensity and a shift of the C=O stretching band, indicating oxidation of phenolic groups during Ag^+ reduction and possible interaction of carbonyl groups with the AgNP surface. TEM analysis showed predominantly quasi-spherical, well-dispersed AgNPs with a narrow size distribution and an average diameter of 8.56 ± 1.61 nm. XRD analysis confirmed a single-phase crystalline face-centered cubic silver structure, while XRF analysis indicated a high silver content of approximately 94.6 wt%. In photocatalytic experiments, MB removal efficiency increased with increasing AgNP dosage and decreased with increasing initial MB concentration due to competitive adsorption and light screening effects. Under optimal conditions (1.5 mg L^{-1} MB, 3% v/v AgNP dosage, and 60 W white LED irradiation), near-complete MB removal (99.9%) was achieved within 420 min. Effective MB degradation was also observed under solar irradiation, demonstrating photocatalytic activity under low-energy light sources.

Conclusions: This study demonstrates that mango leaf extract can serve as an efficient and environmentally friendly bioreducing and stabilizing agent for silver nanoparticle synthesis. The MLE-mediated AgNPs exhibited favorable formation kinetics, well-defined nanoscale characteristics, and high photocatalytic efficiency toward methylene blue degradation under both white LED and solar irradiation, highlighting their potential for sustainable wastewater treatment applications.

Keywords: silver nanoparticles; green synthesis; photocatalyst; methylene blue; degradation

***Corresponding author. E-mail:** nuttawisit@go.buu.ac.th

Introduction

Silver nanoparticles (AgNPs) find a wide range of biomedical applications, including antibacterial, wound-healing, and anticancer properties (Almatroudi, 2020); however, they have also recently gained attention as efficient photocatalysts for organic dye degradation under light irradiation. Upon light excitation, collective oscillations of electron density localized on the AgNP surface, known as surface plasmons, transfer energy to conduction electrons. These excited electrons subsequently interact with oxygen and water to generate reactive oxygen species (ROS), such as superoxide and hydroxyl radicals, which mineralize dyes into non-toxic products (CO_2, H_2O, etc.) without the use of hazardous chemicals (Marimuthu *et al*., 2020). Given these broad applications, environmentally friendly synthesis of AgNPs has become increasingly important. Traditionally, AgNPs are synthesized via chemical reduction using agents such as sodium borohydride or hydrazine; although effective, these methods involve toxic reagents and specialized stabilizers (PVA, PVP, etc.), raising environmental concerns. Consequently, plant-mediated green synthesis has emerged as a sustainable alternative, in which plant extracts rich in phenolic compounds reduce silver ions (Ag^+) to metallic silver (Ag^0) while forming a protective layer that prevents agglomeration and enhances colloidal stability (Gebre, 2023).

This study demonstrates a simple, eco-friendly method for synthesizing colloidal AgNPs using mango leaf extract (MLE) from the Thai Nam Dok Mai cultivar. Mango (*Mangifera indica*) leaves are an abundant agricultural byproduct in Thailand, serving as a low-cost and sustainable precursor material for value-added applications. A major bioactive component of MLE is mangiferin (Figure 1a), a xanthone-based phenolic compound with a C-glucosyl moiety (Chewchinda *et al*., 2021). Its 6,7-OH groups facilitate the reduction of Ag^+ to Ag^0 through electron donation, concurrently forming quinoid species that contribute to AgNP stabilization. A similar electron-donating mechanism has been proposed for the 3′,4′-OH groups in quercetin, a plant flavonoid widely known for its role as a reducing agent for green synthesis (Pardo-Andreu *et al*., 2007; Gebre, 2023). Despite numerous studies on plant-mediated AgNP synthesis, the kinetics of nanoparticle formation and their photocatalytic performance under low-energy LED irradiation remain relatively less explored. Herein, MLE was prepared using water as the sole solvent, enabling a simple and green procedure without the use of organic solvents and ensuring compatibility with the aqueous Ag^+ ions from $AgNO_3$. The influence of synthesis conditions, including incubation temperature, $AgNO_3$ concentration, MLE volume fraction, and pH, on AgNP formation was investigated. The photocatalytic efficiency of the MLE-mediated AgNPs was evaluated via the degradation of methylene blue (MB) under white LED light and solar irradiation (Figure 1b). MB is a common yet toxic cationic dye widely used in textile and biological applications (Oladoye *et al*., 2022). Since MB is chemically

stable and environmentally persistent, its light-driven degradation using green-synthesized AgNPs presents a promising strategy for sustainable wastewater remediation.

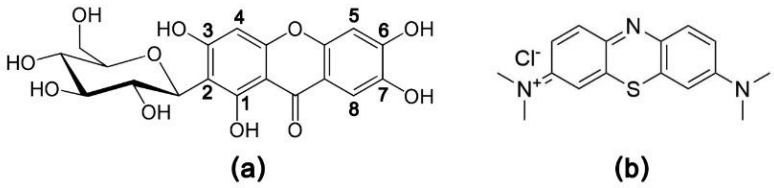

Figure 1 Chemical structures of (a) mangiferin and (b) methylene blue.

Methodology

1. Chemicals and Materials

Silver nitrate ($AgNO_3$, 99.9%, PA grade; POCH) and methylene blue ($C_{16}H_{18}N_3SCl \cdot 2H_2O$, ≥ 95% purity, AR grade; Ajax Finechem) were used as received. Fresh mango leaves (*Mangifera indica* L. cv. Nam Dokmai) were collected in Chonburi, Thailand.

2. Characterization Methods

UV–Vis and FTIR spectra were obtained using an Agilent Cary 3500 UV–Vis spectrophotometer and a PerkinElmer System 2000 FTIR spectrometer, respectively. The crystalline structure and elemental composition were analyzed by X-ray diffraction (XRD, Bruker D2 Phaser) and X-ray fluorescence spectroscopy (XRF, Horiba XGT-9000). Particle morphology was examined using transmission electron microscopy (TEM, Philips Tecnai 20) and scanning electron microscopy (SEM, LEO 1450VP).

3. Preparation of MLE

Fresh mango leaves (600 g) washed with tap water followed by DI water, air-dried overnight, and then oven-dried at 60 °C for 8 h (yielding 150 g, 25% yield). The dried leaves were ground and extracted in 2 L of DI water at 50 °C for 4 h. The mixture was filtered to obtain the amber-colored mango leaf extract (MLE).

4. MLE-Mediated AgNP Synthesis

AgNP synthesis was carried out by reacting $AgNO_3$ (1–7 mM) with MLE (1–30%, v/v) in a total volume of 50 mL. The pH of MLE (3–11) was adjusted using 0.01 M HNO_3 or NaOH solutions. The mixtures were stirred at 20–60 °C using a magnetic stirrer equipped with temperature control. Aliquots (1.5 mL) were collected at predetermined

time intervals to monitor the evolution of the surface plasmon resonance (SPR) band by UV–Vis spectrophotometry. Reaction kinetics were analyzed using a pseudo-first-order model:

$$A_t = A_\infty - (A_\infty - A_0)e^{-k_{obs}t} \quad (1)$$

where A_t, A_0 and A_∞ denote the absorbance of the SPR band at time t, zero, and infinity, respectively. The observed rate constant of AgNP formation (k_{obs}) was determined by nonlinear curve fitting. The temperature dependence of k_{obs} was evaluated using the Arrhenius (Eq. 2) and Eyring (Eq. 3) models (Ghasemi *et al*., 2016):

$$\ln k_{obs} = -\frac{E_a}{R}\left(\frac{1}{T}\right) + \ln A \quad (2)$$

$$\ln\left(\frac{k_{obs}}{T}\right) = -\frac{\Delta H^{\ddagger}}{R}\left(\frac{1}{T}\right) + \ln\left(\frac{k_B}{h}\right) + \frac{\Delta S^{\ddagger}}{R} \quad (3)$$

where R, k_B, h and A denote the gas constant, the Boltzmann constant, the Planck constant, and the pre-exponential factor, respectively. The Arrhenius activation energy (E_a) was determined from the Arrhenius plot ($\ln k_{obs}$ vs. 1/T), while the enthalpy ($\Delta H^{\ddagger}$) and entropy ($\Delta S^{\ddagger}$) of activation were obtained from the Eyring plot ($\ln(k_{obs}/T)$ vs. 1/T). The Eyring activation energy ($\Delta E_a^{\ddagger}$) and Gibbs energy of activation ($\Delta G^{\ddagger}$) were calculated as $\Delta E_a^{\ddagger} = \Delta H^{\ddagger} + RT$ and $\Delta G^{\ddagger} = \Delta H^{\ddagger} - T\Delta S^{\ddagger}$.

5. Photocatalytic MB Degradation Experiments

The synthesis conditions selected from the preliminary studies were scaled up to produce 2 L of AgNP suspension. Excess MLE was removed by centrifugation (8,000 rpm, 5 min), followed by redispersion of the precipitate in DI water using vortexing and ultrasonication. This purification step was repeated twice. The final suspension was stored at 4 °C for photocatalytic experiments. The particle concentration was determined by oven-drying three 4-mL aliquots at 120 °C and averaging the results. Photocatalytic degradation of MB was conducted in an irradiation chamber (Figure 2a) under visible light using either a 60 W or 30 W white LED lamp. Both the 60 W (Figure 2b) and 30 W (Figure 2c) LED lamps showed broad visible-range photon flux distributions with major blue, green, and red components overlapping with typical AgNP SPR absorption, while the 60 W LED lamp provided a higher total photon flux. Reaction mixtures (200 mL) were prepared by mixing appropriate volumes of a 100 mg L^{-1} MB stock solution, the as-prepared AgNP suspension and DI water in a glass cell to achieve target concentrations of 1.5–10 mg L^{-1} MB and 0.5–3% v/v AgNP dosage. After 60 min of dark stirring to reach adsorption–desorption

equilibrium, the mixtures were irradiated. Aliquots (1.5 mL) were withdrawn every 30 min, centrifuged, and the resulting supernatant was analyzed by UV–Vis spectrophotometry. Solar-driven degradation experiments were also conducted in Chonburi (8:00 AM–5:30 PM, April 10, 2025). LED-driven reactions were maintained at 30 ± 3 °C and pH ~7 while the temperature of the sample under natural sunlight ranged from 27 to 36 °C. Degradation kinetics were analyzed using a pseudo-first-order model:

$$A_t = A_0 e^{-k_{deg} t} \quad (4)$$

where A_t and A_0 are the MB peak absorbances at irradiation time and zero, respectively. The apparent rate constant of degradation (k_{deg}) was determined via nonlinear curve fitting. The MB removal efficiency (%R) was calculated as:

$$\%R = \left(\frac{A_0 - A_t}{A_0}\right) \times 100 \quad (5)$$

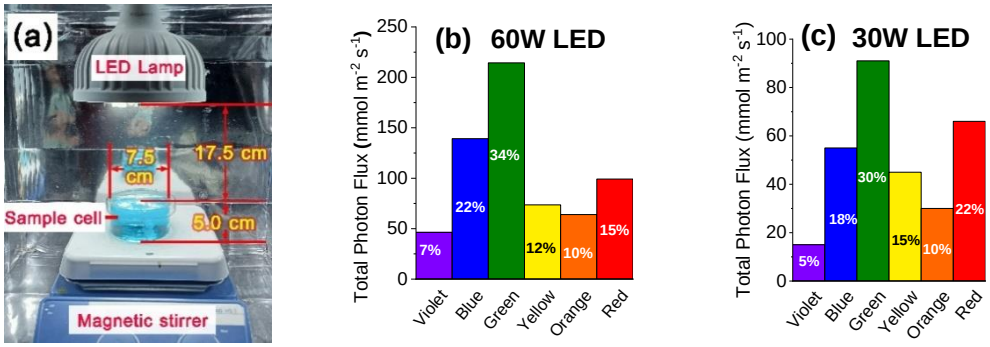

Figure 2 (a) Irradiation chamber for photocatalytic degradation experiments. (b,c) Total photon flux distributions measured in the same chamber configuration: (b) 60 W and (c) 30 W white LED lamps

Results

1. FTIR Analysis of MLE and MLE-Mediated AgNPs

Figure 3 shows the FTIR spectra of MLE and MLE-mediated AgNPs. Several spectral changes were observed upon AgNP formation. The broad O–H stretching band (3400–3280 cm^{-1}) markedly decreased in intensity, whereas the aliphatic C–H stretching region (3000–2800 cm^{-1}) remained relatively unchanged. The C=O stretching band shifted from

1730 to 1740 cm^{-1} with increased intensity. In addition, the aromatic C=C stretching bands (1642–1452 cm^{-1}) showed a decrease in intensity. The C–O stretching bands (1280–1012 cm^{-1}) became less sharp with minor peak shifts.

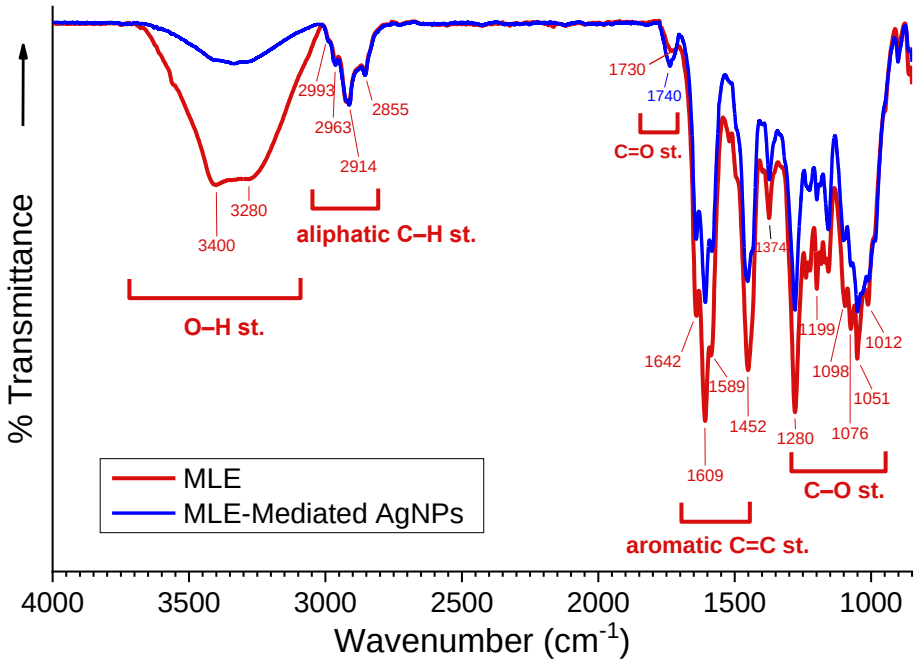

Figure 3 FTIR spectra of MLE and MLE-mediated AgNPs.

Table 1 Observed formation rate constants (k_{obs}) of AgNPs at different incubation temperatures (5 mM $AgNO_3$, 5% v/v MLE and pH 7), together with the corresponding coefficients of determination (R^2), Arrhenius activation energies (E_a), and Eyring activation parameters ($\Delta H^{\ddagger}$, $\Delta S^{\ddagger}$, $E_a^{\ddagger}$, and $\Delta G^{\ddagger}$)

T (°C)	k_{obs} (min^{-1})	R^2	E_a (kJ mol^{-1})	$\Delta H^{\ddagger}$ (kJ mol^{-1})	$\Delta S^{\ddagger}$ (kJ mol^{-1} K^{-1})	$E_a^{\ddagger}$ (kJ mol^{-1})	$\Delta G^{\ddagger}$ (kJ mol^{-1})
20	0.0049	0.9981	26.88	24.36	-0.2057	26.80	84.67
30	0.0074	0.9990				26.88	86.72
45	0.0124	0.9966				27.00	89.81
60	0.0184	0.9948				27.13	92.90
						Mean = 26.95	Mean = 88.52

2. Synthesis Conditions and Formation Kinetics of AgNPs

Figure 4a shows the UV–Vis spectra of the $AgNO_3$–MLE reaction mixture recorded at different incubation times under fixed conditions (5 mM $AgNO_3$, 5% v/v MLE, pH 7, 60 °C). The MLE spectrum (control) exhibited characteristic bands at 317 and 364 nm, consistent with the reported UV–Vis spectrum of mangiferin (Vo *et al*., 2017), while incubation with $AgNO_3$ led to the development of a SPR band for AgNPs at 425 nm with increasing intensity over time, correlating with the color change of the reaction mixture from yellow to reddish-brown (inset images). Figure 4b shows the time-dependent SPR absorbance at different incubation temperatures (20–60 °C), where higher temperatures resulted in faster increases and higher final SPR absorbances. The data were well fitted by a pseudo-first-order kinetic model ($R^2 > 0.99$), with the observed rate constants (k_{obs}) at different temperatures shown in Table 1. The Arrhenius (Figure 4c) and Eyring plots (Figure 4d) both showed good linearity ($R^2 > 0.99$), yielding similar activation energies of 26.88 and 26.95 kJ mol^{-1}, respectively; the entropy of activation ($\Delta S^{\ddagger}$) and Gibbs energy of activation ($\Delta G^{\ddagger}$) are also listed in Table 1.

Figures 4e–4g show the effects of $AgNO_3$ concentration, MLE volume fraction, and pH on AgNP formation under identical incubation conditions (60 °C, 350 min). As shown in Figure 4e, a plateau was observed at $AgNO_3$ concentrations ≥ 5 mM, indicating that the amount of reducing agents present in the 5% v/v MLE fraction was insufficient to completely reduce higher concentrations of Ag^+ ions. This observation was further supported by Figure 4f, where at a fixed $AgNO_3$ concentration of 5 mM, increasing the MLE volume fraction beyond 5% v/v led to a further increase in the SPR absorbance (*i.e*., AgNP concentration), reaching a plateau at approximately 25% v/v. As shown in Figure 4g, the SPR absorbance increased with pH and reached a maximum at pH 9, indicating optimal AgNP formation under mildly alkaline conditions, likely due to enhanced polyphenol deprotonation and increased reducing potency (Martínez *et al.,* 2012). At pH 10–11, the reaction mixture turned turbid white, possibly due to the formation of silver hydroxide–related species that competed with AgNP formation.

3. Characterization of Photocatalytic AgNPs

Based on the trends observed in Figures 4b–4g during the preliminary studies, the synthesis conditions were selected for large-scale AgNP preparation (2 L suspension) for photocatalytic MB degradation. An $AgNO_3$ concentration of 5 mM was maintained for consistency with the preliminary experiments, while an incubation temperature of 60 °C and a reaction time of 350 min were selected to ensure efficient and near-complete Ag^+ reduction. An MLE fraction of 30% v/v and a mildly alkaline pH of 9 were employed to provide an excess of phytochemical reducing agents and enhanced reducing power, respectively. These conditions represented a practically feasible set for AgNP synthesis suitable for photocatalytic applications, rather than an exhaustive parameter optimization.

The AgNP concentration in the suspension, as determined by the drying method, was 0.56 ± 0.15 g L^{-1}. Based on an initial Ag^{+} concentration of 5 mM in a total volume of 2 L, an apparent AgNP yield of ~104% was obtained, which falls within the experimental uncertainty of the gravimetrically determined AgNP concentration. In addition, phytochemical residues bound to the nanoparticle surfaces could have contributed to the mass of the dried particles. TEM analysis (Figures 5a–5c) revealed predominantly quasi-spherical, well-dispersed AgNPs with a narrow size distribution and an average diameter of 8.56 ± 1.61 nm. Individual nanoparticles were not clearly resolved in the SEM image (Figure 5d), whereas XRD analysis (Figure 5e) confirmed the face-centered cubic (fcc) crystal structure of Ag, consistent with the standard crystallographic reference (COD 1100136). XRF analysis (Figure 5f) also indicated a high Ag content of ~94.6 wt%, suitable for photocatalysis.

The apparent kinetic parameters and MB removal efficiencies obtained under all investigated conditions are summarized in Table 2. Figures 6b and 6c show the MB removal efficiency (%R) as a function of irradiation time at different AgNP dosages and initial MB concentrations, respectively. As shown in Figure 6b, negligible MB removal was observed in the absence of AgNPs. In the presence of AgNPs, MB adsorption on AgNP surfaces during the 60 min dark stage was favorable, with the initial adsorption efficiency ($\%R_0$) ranging from 23.8% to 64.2% (see Table 2), while subsequent photocatalytic degradation further increased %R. Under optimal conditions (1.5 mg L^{-1} MB, 3% v/v AgNP dosage, and 60 W white LED irradiation), the removal efficiency after 420 min of irradiation ($\%R_{420}$) reached 99.9%, corresponding to near-complete MB removal.

Table 2 Degradation rate constants (k_{deg}), coefficients of determination (R^2), initial adsorption efficiencies ($\%R_0$), and removal efficiencies after 420 min of irradiation ($\%R_{420}$) for photocatalytic degradation of MB under different conditions.

Initial [MB] (mg L^{-1})	AgNP dosage (% v/v)	Light Source	k_{deg} (min^{-1})	R^2	$\%R_0$	$\%R_{420}$
1.5	3	60 W white LED	1.24×10^{-2}	0.9994	64.2	99.9
3	3	60 W white LED	9.91×10^{-3}	0.9993	56.7	99.6
6	0.5	60 W white LED	2.14×10^{-4}	0.9965	23.8	30.3
	0.75	60 W white LED	7.88×10^{-4}	0.9987	26.1	46.6
	1.5	60 W white LED	4.22×10^{-3}	0.9969	32.8	88.9
	3	60 W white LED	9.08×10^{-3}	0.9988	52.9	99.2
	3	30 W white LED	2.58×10^{-3}	0.9977	52.7	83.8
	3	sunlight	7.27×10^{-3}	0.9976	52.8	97.8
8	3	60 W white LED	8.20×10^{-3}	0.9935	48.9	99.1
10	3	60 W white LED	7.96×10^{-3}	0.9952	47.5	98.7

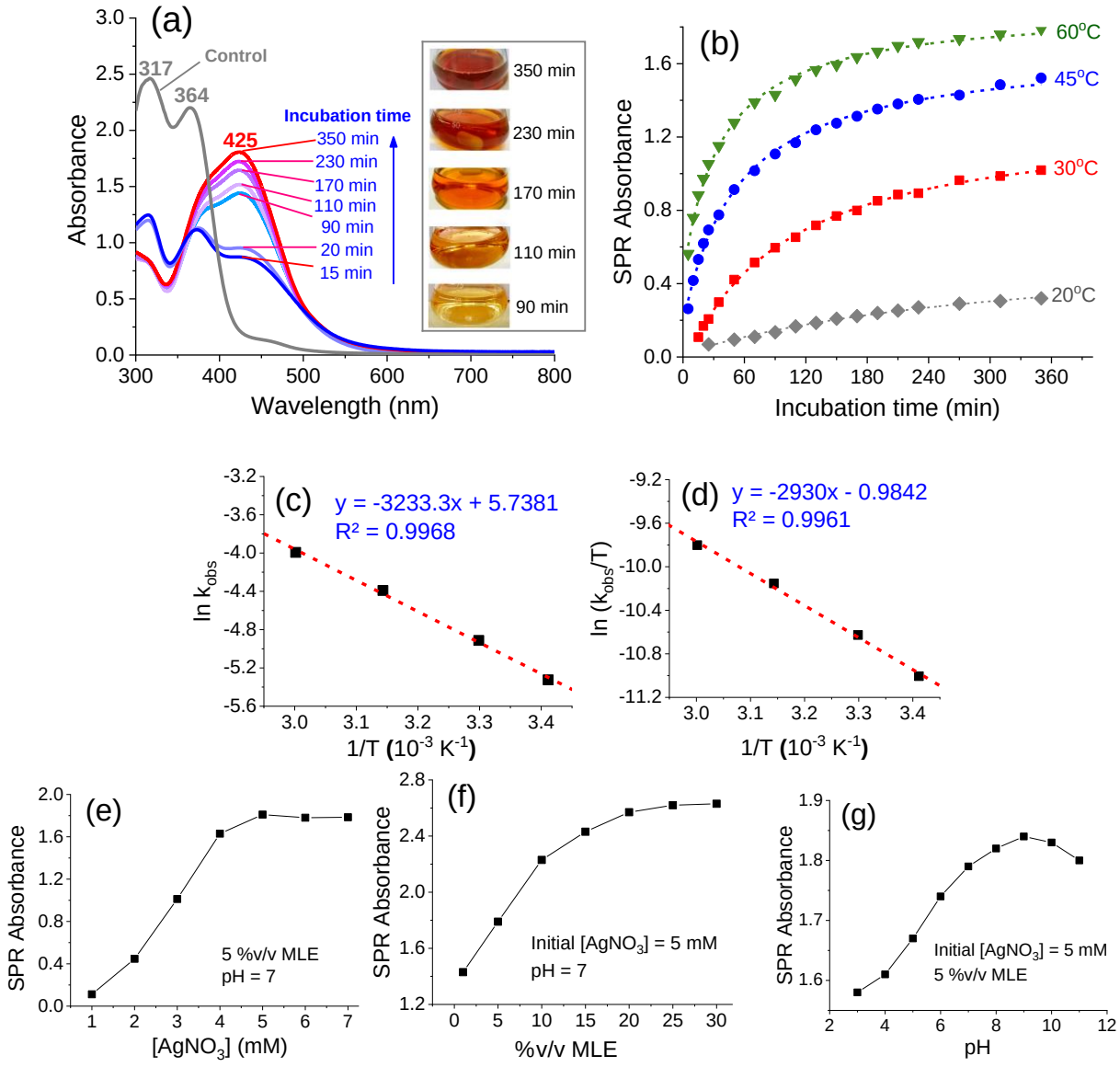

Figure 4 (a) Time-dependent UV–Vis spectra of the $AgNO_3$–MLE mixture under fixed conditions (5 mM $AgNO_3$, 5% v/v MLE, pH 7, 60 °C); inset shows color change during AgNP formation. (b) Evolution of the AgNP SPR band with incubation time at different temperatures. (c) Arrhenius plot. (d) Eyring plot. (e) Effect of $AgNO_3$ concentration on AgNP formation (MLE = 5% v/v, pH 7). (f) Effect of MLE volume fraction on AgNP formation ($AgNO_3$ = 5 mM, pH 7). (g) Effect of pH on AgNP formation ($AgNO_3$ = 5 mM, MLE = 5% v/v).

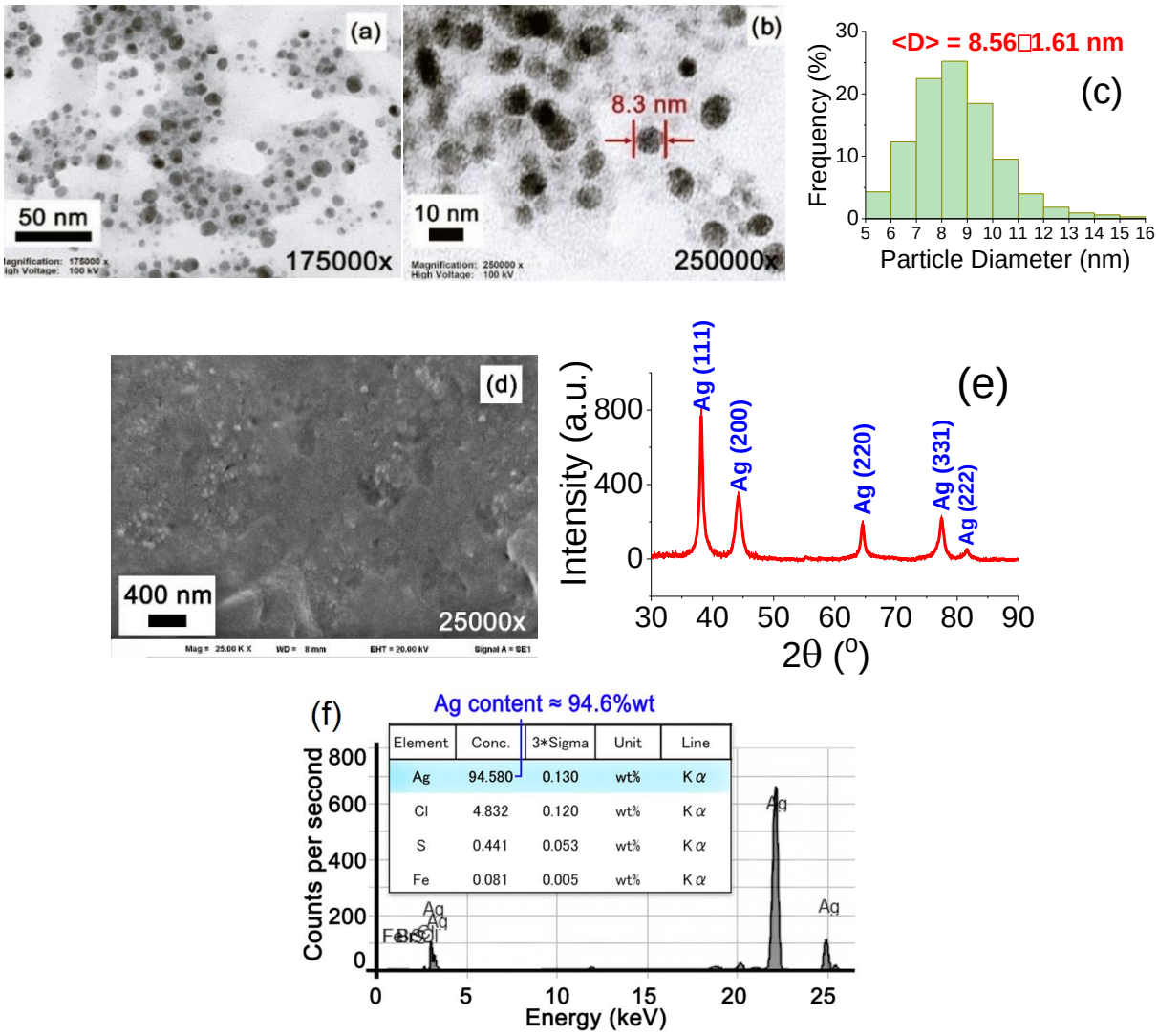

Figure 5 (a,b) TEM images of photocatalytic AgNPs at different magnifications: (a) 175,000x and (b) 250,000x. (c) Size distribution of AgNPs obtained from TEM analysis. (d) SEM image of AgNPs. (e) XRD pattern of AgNPs indexed to the face-centered cubic Ag crystal structure. (f) XRF spectrum of AgNPs.

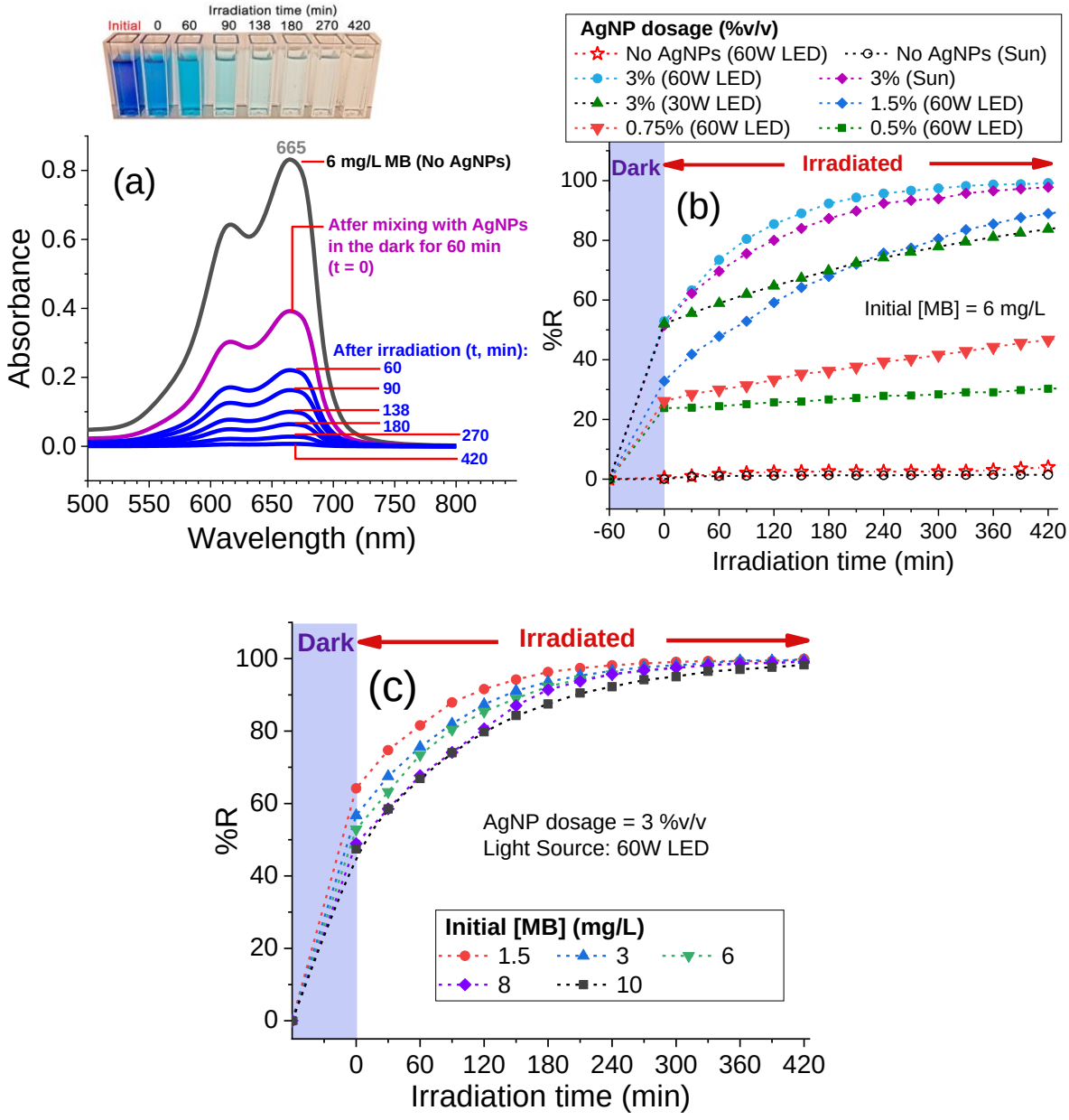

Figure 6 (a) Time-dependent UV–Vis spectra of MB under a 60 W white LED. (b) %R of MB versus time at different AgNP dosages and light sources [initial MB concentration = 6 mg L^{-1}]. (c) %R of MB versus time at different initial MB concentrations under 60 W white LED [AgNP dosage = 3% v/v].

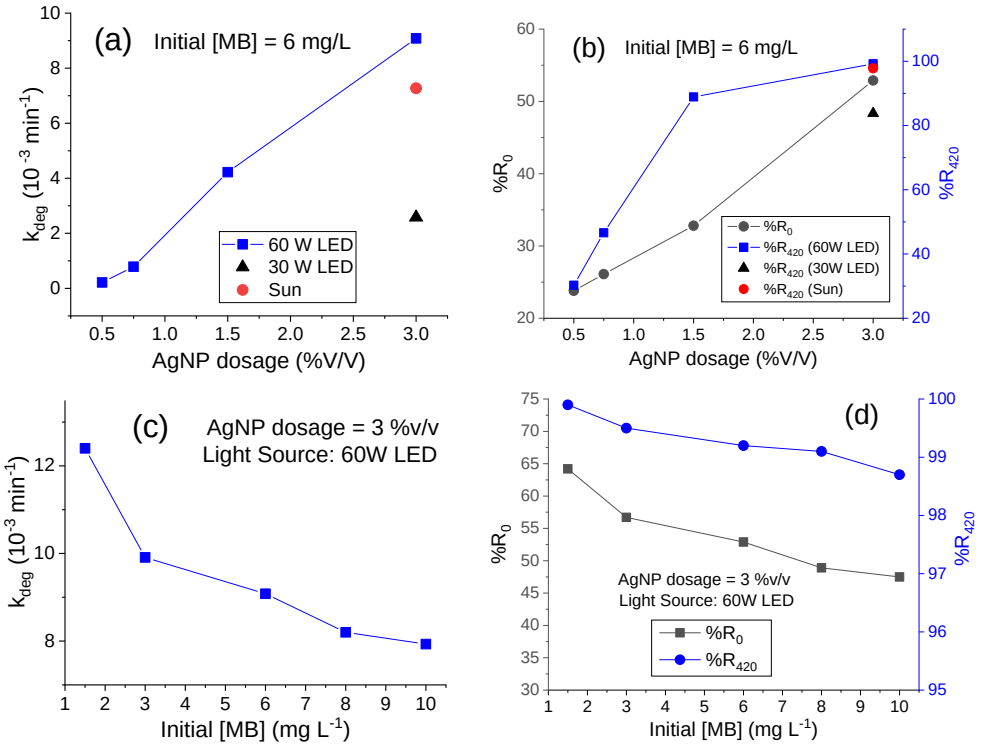

Figure 7 (a) k_{deg} versus AgNP dosage under different light sources [initial MB concentration = 6 mg L^{-1}]. (b) $\%R_0$ and $\%R_{420}$ versus AgNP dosage [initial MB concentration = 6 mg L^{-1}]. (c) k_{deg} versus initial MB concentration under a 60 W white LED [AgNP dosage = 3% v/v]. (d) $\%R_0$ and $\%R_{420}$ versus initial MB concentration under a 60 W white LED [AgNP dosage = 3% v/v].

Figure 7 summarizes the effects of AgNP dosage, initial MB concentration, and light source on the degradation rate constant (k_{deg}), $\%R_0$, and $\%R_{420}$. Figure 7a shows the dependence of k_{deg} on AgNP dosage at a fixed initial MB concentration of 6 mg L^{-1} under different light sources. In all cases, k_{deg} increased with increasing AgNP dosage, reflecting the greater availability of active catalytic sites. Among all light sources, 60 W white LED irradiation resulted in the highest k_{deg} values, whereas reducing the LED power to 30 W caused a pronounced decrease in k_{deg} by ~3.5-fold. Under sunlight, k_{deg} was slightly lower than that obtained under 60 W LED, likely reflecting the lower and fluctuating photon flux. The effects of AgNP dosage on $\%R_0$ and $\%R_{420}$ are shown in Figure 7b. Both parameters increased with increasing AgNP dosage, indicating enhanced initial adsorption and photocatalytic removal efficiency. Similar to the trend observed for k_{deg}, the highest $\%R_{420}$ values were achieved

under 60 W LED irradiation, followed by sunlight and 30 W LED. Figure 7c shows the effects of initial MB concentration on k_{deg} at a fixed AgNP dosage of 3% v/v under 60 W white LED irradiation. Increasing the initial MB concentration from 2 to 10 mg L^{-1} resulted in a gradual decrease in k_{deg}, possibly attributed to increased competition for active sites at higher concentration and/or reduced photon utilization efficiency at higher dye concentrations. Consistently, as shown in Figure 7d, both $\%R_0$ and $\%R_{420}$ decreased with increasing initial MB concentration under the same conditions. The lower removal efficiencies at higher MB concentrations are likely due to light screening effects and/or saturation of adsorption sites on the AgNP surface. Nevertheless, near-complete MB removal was achieved under prolonged irradiation. Under optimal conditions of 1.5 mg L^{-1} MB and 3% v/v AgNP dosage, a maximum removal efficiency of 99.9% was obtained after 420 min of irradiation under a 60 W white LED, resulting from effective initial adsorption ($\%R_0$ = 64.2%) and a high degradation rate ($k_{deg} = 1.24\times10^{-2}$ min^{-1}). Notably, under the same operating conditions, a high removal efficiency of 98.7% was maintained even when the initial MB concentration increased to 10 mg L^{-1}. Although the higher MB concentration markedly reduced adsorption (from 64.2% to 47.5%), the degradation rate decreased only moderately, by ~1.6-fold, leading to comparable final removal efficiencies at sufficiently long irradiation times.

Discussion

1. Role of MLE in AgNP Formation

FTIR spectral changes indicate the involvement of MLE polyphenols in AgNP formation. Reduced O–H stretching intensity suggests significant consumption of phenolic groups during Ag^+ reduction, while the shift and increased intensity of the C=O band are consistent with oxidation of these moieties and possible interaction with the Ag surface. Variations in aromatic C=C and C–O bands further reflect modification of the polyphenolic framework. The obtained AgNPs were well-dispersed, quasi-spherical particles with a narrow size distribution, confirming the effectiveness of the MLE-mediated route.

2. AgNP Formation Kinetics

The time-dependent evolution of the SPR band reflected progressive AgNP formation via Ag^+ reduction. In the presence of an excess of reducing agents, the observed pseudo-first-order kinetics were in agreement with several previous studies (Mushran *et al*., 1974; Ewais, 2014; Kumar *et al*., 2022). The increase in k_{obs} with temperature indicated a thermally activated process, with Arrhenius and Eyring analyses yielding similarly low activation energies (~27 kJ mol^{-1}), comparable to the reported value (~20 kJ mol^{-1}) for polyol-mediated AgNPs (Liu *et al*., 2016). The negative $\Delta S^{\ddagger}$ suggested the formation of an ordered transition state, likely involving coordination between Ag^+

ions and phytochemical ligands present in MLE. Despite the low $\Delta H^{\ddagger}$, the relatively high $\Delta G^{\ddagger}$ across the studied temperature range suggested that the AgNP formation rate was primarily governed by the entropic cost associated with molecular organization at the transition state.

3. Performance of AgNPs in MB Removal

Table 3 compares MB removal efficiencies of green-synthesized AgNPs and AgNP-based composites reported in selected recent studies under various conditions and light sources with those of the present study, all at an initial MB concentration of 10 mg L^{-1}. Previous studies generally achieved high MB removal under stringent conditions, including high-power light sources (250–400 W), high catalyst dosages (≥0.1–2 g L^{-1}), acidic pH, long irradiation times, or composite photocatalysts, whereas the present study achieved 98.7% MB removal using a low AgNP dosage (3% v/v) under a low-power 60 W household white LED, albeit with a longer irradiation time (420 min).

Table 3 MB removal efficiencies of AgNP-based photocatalysts synthesized with different bioreducing agents

Catalyst	Bioreducing Agent	Light Source	Catalyst Dose	%R[(a)]	Reference
AgNPs	*A. officinarum* rhizome extract	400 W Visible and UV lamps	10 mg L^{-1} (dry particles added)	80% (120 min, Visible) 38% (120 min, UV);	Lia *et al*., 2020
AgNPs	Honey	Sunlight	0.1 g L^{-1} (dry particles added)	90% (24 h, pH 2); 35% (24 h, pH 6)	Al-Zaban *et al*., 2021
AgNPs	*A. flavus* strain	250 W Halogen lamp	~2 g L^{-1} (dry particles added)	66.5% (%R_0); 86.4% (200 min)	Foud *et al*., 2022
AgNPs	Tea leaf extract	Sunlight	2% v/v (suspension added, equiv. to ~5 mg L^{-1} AgNPs)	95% (72 h)	Trieu, *et al*., 2023
Ag/TiO_2 composite	Mangosteen pericarp extract	50 W LED Lamp	0.5 g L^{-1} (dry particles added)	97% (90 min)	Yuwono, *et al*., 2024
AgNPs	*Centella asiatica* leaf extract	Sunlight	0.1 g L^{-1} (dry particles added)	90% (120 min)	Arulnangai *et al*., 2025
AgNPs	Tomato leaf extract	Sunlight	0.17 g L^{-1} (dry particles added)	83% (80 min)	Tooba *et al*., 2026
AgNPs	Mango leaf extract (MLE)	60 W White LED lamp	3% v/v (suspension added, equiv. to ~17 mg L^{-1} AgNPs)	47.5% (Dark); 74.0 (90 min); 79.8 (120 min); 98.7 (420 min)	The present study

(a) Reported conditions are shown in parentheses as provided in the original references

Conclusions

XRD and XRF analyses confirmed that the obtained AgNPs exhibited a single-phase crystalline fcc silver structure with a silver content of ~94.6 wt%. The colloidal MLE-mediated AgNPs exhibited notable efficiency in

removing MB from water via initial adsorption and subsequent photocatalytic degradation under white LED and solar irradiation. MB removal efficiency increased with AgNP dosage and decreased with increasing initial MB concentration due to reduced adsorption capacity and light shielding effects. Under optimized conditions (1.5 mg L^{-1} MB, 3% v/v AgNP dosage, pH ~7, 60 W white LED), a maximum MB removal efficiency of 99.9% was achieved after 420 min of irradiation. Comparison with recent studies demonstrates that effective MB removal is attainable under milder and less energy-intensive conditions using MLE-mediated AgNPs, highlighting the potential of this system for low-energy wastewater treatment applications. Future studies may further investigate catalyst stability, recyclability, and photocatalytic mechanisms to support practical environmental applications.

References

Almatroudi, A. (2020). Silver nanoparticles: synthesis, characterization and biomedical applications. *Open Life Sciences*, *15*(1), 819-839.

Al-Zaban, M.I, Mahmoud, M.A., & AlHarbi, M.A. (2021). Catalytic degradation of methylene blue using silver nanoparticles synthesized by honey. *Saudi Journal of Biological Sciences, 28*, 2007-2013.

Arulnangai, R., Ganesamoorthy, R., Mohamed, V. B. H., Vivekanand, P. A., Kavitha, P., Kavitha, P., & Thirugnanasambandham, K. (2025). Green synthesis of silver nanoparticles from *Centella asiatica* and its application in photodegradation of methylene blue dye in paper industry effluent. *Cleaner Water, 4*, 100179(1-8).

Chewchinda, S., Suriyaphan, O., Kanchanadumkerng, P., Sato, H., & Hirunpanich Sato, V. (2021). Comparison of Antioxidant and α-glucosidase inhibitory activities in different cultivars of five mango (*Mangifera Indica* L.) leaf extracts. *Chiang Mai University Journal of Natural Sciences, 20*(1), e2021014(1-16).

Ewais, H. A. (2014). Kinetics and mechanism of the formation of silver nanoparticles by reduction of silver (I) with maltose in the presence of some active surfactants in aqueous medium. *Transition Metal Chemistry, 39*, 487–493.

Foud, A., Awad, M. A., AL-Faifi, Z. E., Gad, M. E., Al-Khalaf, A. A., Yahya, R., & Hamza, M. F. (2022) *Aspergillus flavus*-mediated green synthesis of silver nanoparticles and evaluation of their antibacterial, anti-candida, acaricides, and photocatalytic activities. *Catalysts*, *12,* 462(1-19).

Gebre, S. H. (2023). Bio-inspired synthesis of metal and metal oxide nanoparticles: the key role of phytochemicals. *Journal of Cluster Science, 34*, 665-704.

Ghasemi, Z., Younesi, H., & Zinatizadeh, A. A. (2016). Kinetics and thermodynamics of photocatalytic degradation of organic pollutants in petroleum refinery wastewater over nano-TiO_2 supported on Fe-ZSM-5. *Journal of the Taiwan Institute of Chemical Engineers*, *65*, 357-366.

Kumar, I., Gangwar, C., Yaseen, B., Pandey, P. K., Mishra, S. K. , & Naik, R. M. (2022). Kinetic and mechanistic studies of the formation of silver nanoparticles by nicotinamide as a reducing agent. *ACS Omega, 7*(16), 13778–13788.

Lia, J. F., Liu, Y.-C., Chokkalingam, M., Rupa, E. J., Mathiyalagan, R., Hurh, J., Ahn, J. C., Park, J. K., Pu, J. Y., & Yang, D. C. (2020). Phytosynthesis of silver nanoparticles using rhizome extract of *Alpinia officinarum* and their photocatalytic removal of dye under UV and visible light irradiation. *Optik, 208*, 164521(1-7).

Liu, Q., Gao, M.-R., Liu, Y., Okasinski, J. S., Ren, Y., & Sun, Y. (2016). Quantifying the nucleation and growth kinetics of microwave nanochemistry enabled by in situ high-energy x-ray scattering. *Nano Letters*, *16(1)*, 715–720.

Marimuthu, S., Antonisamy, A. J., Malayandi, S., Rajendran, K., Tsai, P.-C., Pugazhendhi, A., & Ponnusamy, V. K. (2020). Silver nanoparticles in dye effluent treatment: A review on synthesis, treatment methods, mechanisms, photocatalytic degradation, toxic effects and mitigation of toxicity. *Journal of Photochemistry and Photobiology B*: *Biology*, *205*, 111823(1–13).

Martínez, A., Hernández-Marin, E., & Galano, A. (2012). Xanthones as antioxidants: A theoretical study on the thermodynamics and kinetics of the single electron transfer mechanism. *Food & Function, 3*, 442–450.

Mushran, S. P., Agrawal, M. C., Mehrotra, R. M., & Sanehi, R. (1974). Kinetics and mechanism of reduction of silver (I) by ascorbic acid. *Journal of the Chemical Society, Dalton Transactions, 14*, 1460–1462.

Oladoye, P. O., Ajiboye, T. O., Omotola, E. O., & Oyewola, O. J. (2022). Methylene blue dye: Toxicity and potential elimination technology from wastewater. *Results in Engineering, 16*, 100678(1-17).

Pardo-Andreu, G. L., Cavalheiro, R. A., Dorta, D. J., Naal, Z., Delgado, R., Vercesi, A. E., & Curti, C. (2007). Fe(III) shifts the mitochondria permeability transition-eliciting capacity of mangiferin to protection of organelle. *Journal of Pharmacology and Experimental Therapeutics, 320(2),* 646–653.

Tooba, Assad, N., Laila, M.B., Iqbal, R.M.F., Manahil, L., Iqbal, J., Naeem-ul-Hassan, M., Khuram, A., Assad, Y., Khan, M.N., Hussain, S., Kaplan, A., Al-Mohaimeed, A.M. ,& Abid, I. (2026). Green synthesis of silver nanoparticles using *Solanum lycopersicum* leaves extract for highly selective detection of mercury ions and photocatalytic degradation of methylene blue. *Discover Nano, 21*(14), 1-31.

Trieu, Q.-A., Le, C. T. B., Pham, C. M., & Bui, T. H. (2023). Photocatalytic degradation of methylene blue and antibacterial activity of silver nanoparticles synthesized from Camellia sinensis leaf extract. *Journal of Experimental Nanoscience, 18*(1), 2225759(1-18).

Vo, T. H. T., Nguyen, T. D., Nguyen, Q.H., & Ushakova, N. A. (2017). Extraction of mangiferin from the leaves of the mango tree *Mangifera indica* and evaluation of its biological activity in terms of blockade of alpha-glucosidase. *Pharmaceutical Chemistry Journal, 51*(9), 806–810.

Yuwono, A. H., Septiningrum, F., Dhaneswara, D., Sofyan, N., Suwartha, N., Lalasari, L. H., Maulana, F. A., Nurhidayah, E., & Barep, A. L. (2024). Investigation of methylene blue dye degradation using green synthesized mesoporous silver-titanium. *South African Journal of Chemical Engineering*, *50*, 415–426.